# Structure and stability of arsenate adsorbed on α-$Al_2O_3$ single-crystal surfaces investigated using grazing-incidence EXAFS measurement and DFT calculation

*Meiyi Zhang, Guangzhi He, Gang Pan**

Research Center for Eco-Environmental Sciences, Chinese Academy of Sciences, Beijing 100085, People's Republic of China

E-mail: myzhang@rcees.ac.cn, gzhhe@rcees.ac.cn, gpan@rcees.ac.cn

*Corresponding author. Phone: +86-10-62849686; Fax: +86-10-62849686; E-mail: gpan@rcees.ac.cn

**Abstract:** Direct characterization of contaminants on single-crystal planes is required because the specific adsorption characteristics on different exposed crystal planes constitute their actual behavior at water-mineral interfaces in aquifers. Here, the structure and stability of arsenate on α-$Al_2O_3$ (0001) and $(11\bar{2}0)$ surfaces were characterized by using a combination of grazing-incidence extended X-ray absorption fine structure (GI-EXAFS) spectra and periodic density functional theory (DFT) calculation. The combined results indicated that arsenate was mainly adsorbed as inner-sphere monodentate and bidentate complexes on both surfaces, but the orientational polar angles on the (0001) surface were commonly 10~20° greater than that on the $(11\bar{2}0)$ surface. The DFT calculation showed that the large polar angle was more favorable for arsenate stabilized on the alumina surfaces. Based on the spectroscopic and computational data, the dominant bonding modes of arsenate on the two crystal planes of α-$Al_2O_3$ were identified as bidentate binuclear structures, and the (0001) surface displayed a stronger affinity toward arsenate.

**Keywords:** surface complex; molecular orientation; structure-stability relationship; GI-EXAFS; density functional theory

## 1. Introduction

The persistence of arsenic in soil and aquatic environments has been ranked as a global environmental problem due to its toxic impact on human health (Oremland and Stolz, 2003). Adsorption of arsenic at the solid-water interface is one of the dominate effects responsible for water treatment and soil decontamination (Jing et al., 2005; Mohan and Pittman, 2007; Singer et al., 2013). Detailed information about the structure and stability of arsenic on solid surfaces is essential for understanding its fate in the environment and developing high-performance adsorbents (van Genuchten et al., 2012).

Over the past two decades, extended X-ray absorption fine structure (EXAFS) spectroscopy has been developed as one of the most important technologies for determining the microstructure of environmental contaminants on solid surfaces (Arai et al., 2001; Duarte et al., 2012; van Genuchten et al., 2012; Waychunas et al., 1993). Most existing EXAFS studies are carried out using powder substrates, where all types of crystal planes may be mixed and expose to the adsorption process. The multiple surface terminations and extensive defects of mineral powder may produce a large number of different adsorption sites (Daniels et al., 2001). Therefore, the structural data obtained from standard powder EXAFS experiment are essentially the average over all values from different exposed crystal planes. To avoid these problems, the application of structurally well-defined single-crystal substrates is needed (Catalano et al., 2005; Singer et al., 2012; Waychunas et al., 2005). Direct characterization of the structure and bonding properties on specific crystal planes is required to conclusively unveil the interaction of arsenic species with adsorbent powders.

Grazing-incidence EXAFS (GI-EXAFS) is a significant development of EXAFS technique, which utilizes well-characterized single-crystal samples (Singer et al., 2012). The application of

crystallographically anisotropic substrate and polarized X-ray beam allows GI-EXAFS to provide more structural information (interatomic distance, coordination number and polar angle) toward the oriented absorbates (Waychunas et al., 2005). These advantages provide the opportunity to obtain direct information about the structure of contaminant molecules on different exposed crystal planes, which may trigger wide applications of GI-EXAFS in environmental geochemistry and geo-engineering as synchrotron facilities are improving. Density functional theory (DFT) calculation can provide a detailed characterization of adsorbate molecules at solid surfaces, including structure, bonding, and energy (Duarte et al., 2012; He et al., 2011). The combination of GI-EXAFS measurement with DFT calculation enables analysis of the structure and stability characteristics of arsenic species on specific crystal planes.

Aluminum is one of the most abundant metals in the earth, and Alumina has been recognized as a very efficient adsorbent for the removal of arsenic from waters (Mohan and Pittman, 2007). α-$Al_2O_3$ is the most stable phase of alumina with a well-determined structure, and an excellent model system for understanding the transport mechanisms of contaminants on Al-(hydr)oxides (Catalano et al., 2008; Trainor et al., 2001). Both (0001) and $(11\bar{2}0)$ planes are stable terminations of α-$Al_2O_3$ surfaces (Lockwood et al., 2008). However, there have been few studies of surface complexation reactions on $(11\bar{2}0)$ plane compared to (0001) and $(1\bar{1}02)$ planes.

Here, we present a combined GI-EXAFS and DFT calculation investigation to study the structure and stability of As(V) adsorbed on the (0001) and $(11\bar{2}0)$ surfaces of α-$Al_2O_3$. In the GI-EXAFS experiment, two directions of the X-ray electric vector, parallel and perpendicular to the substrate, were used to determine the structure of As(V) bonded to both surfaces. Periodic DFT calculations were performed to describe the binding and energetic characteristics of arsenate on α-$Al_2O_3$ surfaces.

## 2. Experimental and Computational Methods

### *2.1. Sample preparation*

Highly polished 25×25×0.43 $mm^3$ α-$Al_2O_3$ (0001) and $(11\bar{2}0)$ single crystals were obtained commercially from Shanghai Daheng Optics and Fine Mechanics Co., Ltd, China. The orientations were checked using High accuracy X-ray single crystal orientation instrument (DX-4A, Dandong, China) and were found to be perfectly oriented to the resolution limits of the equipment (~2 Å). The roughness was assessed with AFM (Veeco Dimension 3100) and was found to be ≤5 Å rms. Prior to initial use, the crystals were washed in $10^{-4}$ mol/L nitric acid and ethanol followed by multiple rinses with MilliQ water (resistivity 18 MΩ.cm). The crystals were then equilibrated with 1 mmol/L $Na_2HAsO_4$ solution at pH 7.0 for 2h, with a 0.01 mol/L $NaNO_3$ background electrolyte. The pH of the reaction system was constantly monitored and adjusted to the desired value of 7.0 with 0.1 mol/L NaOH or 0.1 mol/L $HNO_3$. All chemicals used for solution preparation were of reagent grade quality.

### *2.2. GI-EXAFS data collection and analysis*

Grazing-incidence EXAFS experiments were performed on the beamline BL14W1 at the Shanghai Synchrotron Radiation Facility (SSRF). A purposely built apparatus (Fig. S1 in the Supporting Information) consists of a carriage that holds the sample stage, with motor drives for positioning the sample over 5 degrees of freedom (Waychunas et al., 2005). A wet arsenate-loaded crystal sample was placed on the sample stage for GI-EXAFS measurements. The carriage can be rotated around the incident X-ray beam to set the angle of the X-ray electric vector polarization plane with respect to the sample surface. Ionization chamber detectors were mounted on both sides of the sample for transmission absorption data collection, and a 4-channel Si drift detector (SDD, Canberra Industries, Inc.) was used to collect fluorescence signals. The angle of the incident X-rays (beam diameter of ~30

μm) to the single-crystal surfaces was set to 0.16°, which is less than the critical angle of α-$Al_2O_3$ at the energy position of As K-edge (0.19º) (Klockenkämper, 1997). The experimental uncertainty on the incident angle of X-rays is ≤ 0.01°. The GI-EXAFS measurements were carried out using two scan modes with the electric vector respectively parallel and perpendicular to the single-crystal substrate. The crystal samples were mounted in a Teflon cell and sealed with Mylar film during the GI-EXAFS experiment. During the data collection, the sample cell was continuously purged with a constant flow of water-saturated inert gas (ultrapure $N_2$) to keep the crystals moist, which has been widely used in GI-EXAFS experiments (Furnare et al., 2005; Waychunas et al., 2005). An average of 3 scans was performed to achieve suitable single/noise, and no obvious change in spectral data was observed during the 3 scans.

The spectral data were processed using WinXAS 3.1 software package (Ressler, 1998). A linear function fit for the pre-edge region and a second-order polynomial fit in the post-edge region were used to yield the normalized and background-corrected spectra. Subsequently, the normalized spectra were converted to frequency ($k$) space using a cubic spline function and weighted by $k^3$. The $k^3\chi$ (k) spectra (typically range from 2.2 to 12.4 $Å^{-1}$) were Fourier-transformed (FT) to $R$ space using a Bessel window function with smoothing parameter of 4. Theoretical phase shift and amplitude functions for single- and multiple-scattering paths were calculated by ab initio Feff 9.0 code (Ankudinov et al., 1998) using the cluster of scorodite ($FeAsO_4 \cdot 2H_2O$) with the Fe atom replaced by Al atom. This method has been successfully used in the study of arsenic species adsorption on Al-(hydr)oxide surfaces (Arai et al., 2001). An amplitude reduction factor ($S_0^2$) of 0.9 was used in data-fitting procedure (Grafe et al., 2008; Jing et al., 2005). We used 4, 2, and 1 as the starting values of the As-O coordination number ($CN_{As\text{-}O}$), the $CN_{As\text{-}Al}$ for binuclear complex, and the $CN_{As\text{-}Al}$ for mononuclear

115 complex in the data fitting, to obtain estimated values for interatomic distances ($R$), DW factors $\sigma^2$,
116 and $\Delta E_0$. Then the $R$, $\sigma^2$, and $\Delta E_0$ were fixed to obtain the estimated $CN$ for each shell. The estimated
117 values of $CN$, $R$, $\sigma^2$ and $\Delta E_0$ were then used for a sequential fitting that recorded the reduction of the
118 residual until the best fit was obtained. A single $\Delta E_0$ was applied to all shells and allowed to float
119 during the fitting. Finally, all the parameters ($CN$, $R$, $\sigma^2$) for each backscattering paths were allowed to
120 vary. The goodness of fit is evaluated by the residual, defined as

121 $$\text{Residual [\%]} = \frac{\sum_{i=1}^{N} | y_{\exp}(i) - y_{theo}(i) |}{\sum_{i=1}^{N} | y_{\exp}(i) |} .100$$

122 with N the number of data points, $y_{exp}$ and $y_{theo}$ experimental and theoretical data points,
123 respectively (Ressler, 2009). It has been reported that reasonable EXAFS results were generally
124 obtained for arsenate adsorption on Fe- and Al-oxides when the residuals were less than 20% (Grafe
125 and Sparks, 2005; Tang and Reeder, 2009). The As-Al shells were respectively regarded as a single
126 shell and two subshells, and fitted using one single As-Al scattering path and two different As-Al
127 paths. The results showed that the residuals of single-shell fits were commonly larger than that of
128 two-subshell fits (see Fig. S2 in the Supporting Information), which experimentally confirmed the
129 multiple coordination structures (i.e., the coexistence of two dominant adsorption configurations) of
130 arsenate on α-$Al_2O_3$ surfaces. The experimental spectra were also fitted using the As-As scattering
131 path and the As-O-O-As multiple scattering path (Fig. S3 and Fig. S4 in the Supporting Information).
132 The increasing residuals indicated that the As(V)-bearing solid phase did not exist in the adsorption
133 system considered here (1 mmol/L, pH 7.0), and no significant improvement was found by adding
134 multiple scattering effects to the fitting. Therefore, to reduce the number of free parameters during the
135 fitting, As-As scattering path and multiple scattering path were not employed in the final fitting.

136 *2.3. Computational settings*

137 The calculations were carried out using the generalized gradient approximation (GGA) with the
138 functional parameterized by Perdew, Burke and Enzerhof (PBE) (Perdew et al., 1996) as implemented
139 in the DMol3 module of Materials Studio package (Accerlys Software Inc.) (Delley, 1990; Delley,
140 2000). In the spin-restricted DFT calculations, the geometrical and electronic structures of Al-$AsO_4$
141 complexes were computed under periodic boundary conditions (PBC). The valence electron wave
142 functions were expanded using a double numerical plus polarization (DNP) basis set which includes a
143 polarized d-function for non-hydrogen atoms and p-function for hydrogen atoms (Delley, 2000). The
144 size of the DNP basis set is comparable to Gaussian 6-31G (d, p), but the DNP is more accurate than a
145 Gaussian basis set of the same size (Inada and Orita, 2008). The core electrons were described by
146 effective core potentials (ECP) (Hay and Wadt, 1985). The global orbital cutoff was taken to be 4.8 Å
147 (fine standard in DMol3). The conductor-like screening model (COSMO) was applied to simulate the
148 water solvent environment (Klamt, 1995; Klamt and Schuurmann, 1993). The fine quality mesh size
149 was employed for the numerical integration. The Brillouin zone was sampled with a 2×2×1
150 Monkhorst-Pack k-point grid for the structural optimization. A Fermi smearing of 0.005 hartree (1
151 hartree = 27.2114 eV = 2625.5 kJ/mol) was used to improve convergence efficiency (Delley, 1995).
152 The geometry optimization convergence tolerances of the energy, gradient, and displacement were
153 $1\times10^{-5}$ Hartree, $2\times10^{-3}$ Hartree $Å^{-1}$, and $5\times10^{-3}$ Å, respectively.

154 *2.4. Computational model*

155 The unit cell of α-$Al_2O_3$ was optimized before construction of the supercell, and the calculated
156 lattice constants ($a$ = 4.759 Å, $c$ = 12.991 Å) agreed favorably with the experimental values ($a$ = 4.766
157 Å, $c$ = 13.010 Å) and other theoretical works (Montanari et al., 2006). The surface in Fig. 1a is the

most stable among the three cleavage planes of α-$Al_2O_3$ (0001) surface (Mason et al., 2009; Walters et al., 2000) and was used in this study. From existing studies, a slab contained five repeated $Al_2O_3$ layers generally allows a good description to the surface adsorption of adsorbate molecules (Duarte et al., 2012; Hellman and Gronbeck, 2009). Therefore, the slab consisting of five $Al_2O_3$ layers was used here as the surface model (see Fig. 1). The supercell expansions and spatial dimensions of each surface slab are listed in Table 1. Surface hydroxylation of α-$Al_2O_3$ will occur in the presence of water, and forms the reactive surface sites (Hass et al., 1998; Wang et al., 2000). Therefore, the surface of the slab was hydroxylated in the calculation of arsenate surface complexation. During the geometrical optimization, the arsenate and the top three $Al_2O_3$ layers (i.e., six atomic planes) were allowed to relax, and the bottom two $Al_2O_3$ layers were fixed at equilibrium crystal lattice sites to simulate bulk conditions (Hellman and Gronbeck, 2009; Ojamae et al., 2006; Ranea et al., 2008). A vacuum thickness of 15 Å normal to the surface was used to eliminate spurious interactions between the adsorbate and the periodic image of the bottom layer of the slabs (Roscioni et al., 2013). A counter positive charge was automatically added by DMol3 package during the calculations in order to keep the neutrality of the whole model to avoid divergence in the electrostatic energy (Makov and Payne, 1995).

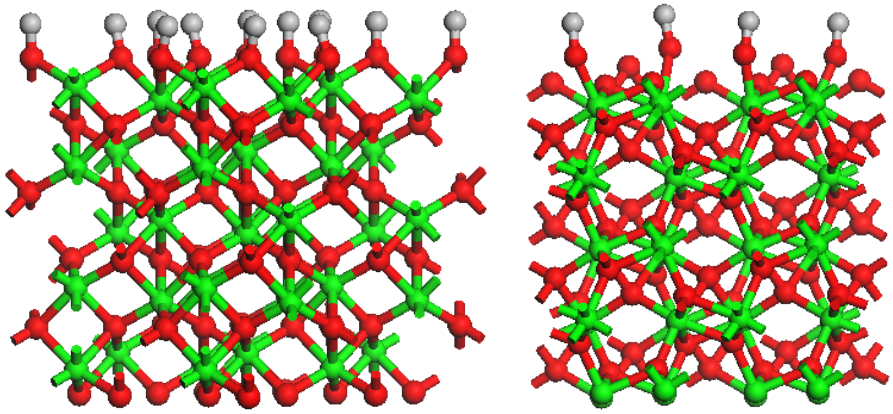

**a** (0001) **b** (11$\bar{2}$0)

**Fig. 1.** Side views of the hydroxylated α-$Al_2O_3$ (0001) (a) and (11$\bar{2}$0) (b) surface models used in DFT calculation. Green, red, and gray circles denote aluminum, oxygen, and hydrogen atoms, respectively.

**Table 1.** Supercell expansions and lattice parameters used to construct α-$Al_2O_3$ (0001) and (11$\bar{2}$0) surface models

| Surface | Expansion | $L_x$ (Å) | $L_y$ (Å) | $L_z$ (Å) | Area/Å$^2$ | $N_{Al2O3}$ |
|---|---|---|---|---|---|---|
| (0001) | 2×2 | 9.52 | 9.52 | 10.83 | 90.63 | 22 |
| (11$\bar{2}$0) | 1×2 | 7.00 | 10.26 | 11.17 | 71.82 | 20 |

Test calculations with larger orbital cutoff (5.2 Å) and denser *k*-point sampling (3×3×2) show almost no change in the structural and energetic properties. Negligible difference to the adsorption geometries (<0.01 Å) and binding energies (<5 kJ/mol) was found when the relaxed $Al_2O_3$ layers increased from 3 to 4 (see Table S1 in the Supporting Information), indicating that the structural parameters and relative energies of arsenate adsorption have converged when the relaxed $Al_2O_3$ layers increased to 3 (i.e., six atomic planes). These tests verified that the present computational settings and models were reliable for describing the properties of arsenate on α-$Al_2O_3$ surfaces.

## 3. Results and Discussion

### *3.1. GI-EXAFS analysis*

188 The $k^3$-weighted and Fourier transform spectra of As K-edge GI-EXAFS for the adsorption samples
189 of arsenate on α-$Al_2O_3$ (0001) and $(11\bar{2}0)$ single-crystal surfaces are shown in Fig. 2. GI-EXAFS
190 fitting data are presented in Table 2. Based on our fitting results, we estimated the accuracies of the
191 As–O shell to be ±0.005 Å for interatomic distance ($R$) and ±5% for coordination number ($CN_{As\text{-}O}$).
192 The estimated errors were ±0.02 Å, ±0.03 Å and ±20% for $R$ of As–Al first subshell, $R$ of As–Al
193 second subshell and $CN_{As–Al}$, respectively. The GI-EXAFS fitting results showed that the first
194 coordination shell of the arsenic atom consisted of four oxygen atoms at a distance of ~1.69 Å, which
195 is in good agreement with the literature (He et al., 2009; Waychunas et al., 2005). As a result of the
196 high symmetry of $AsO_4$ tetrahedron, no obvious difference in $CN_{As\text{-}O}$ (Table 2) was observed between
197 both polarized scans (electric vector parallel and perpendicular to the substrate). For (0001) plane, the
198 two As-Al distances obtained from GI-EXAFS analysis (3.11±0.02 and 3.33±0.03 Å) agreed well with
199 DFT-calculated values of bidentate binuclear (BB) complex (3.07 Å) and monodentate binuclear (MB)
200 complex (3.30 Å), respectively (Table 3). The two experimentally measured As-Al distances on $(11\bar{2}0)$
201 plane (3.04±0.02 Å and 3.20±0.03 Å) were consistent with the theoretical values of BB (3.07 Å) and
202 monodentate mononuclear (MM, 3.21 Å) complexes (see Table 3).

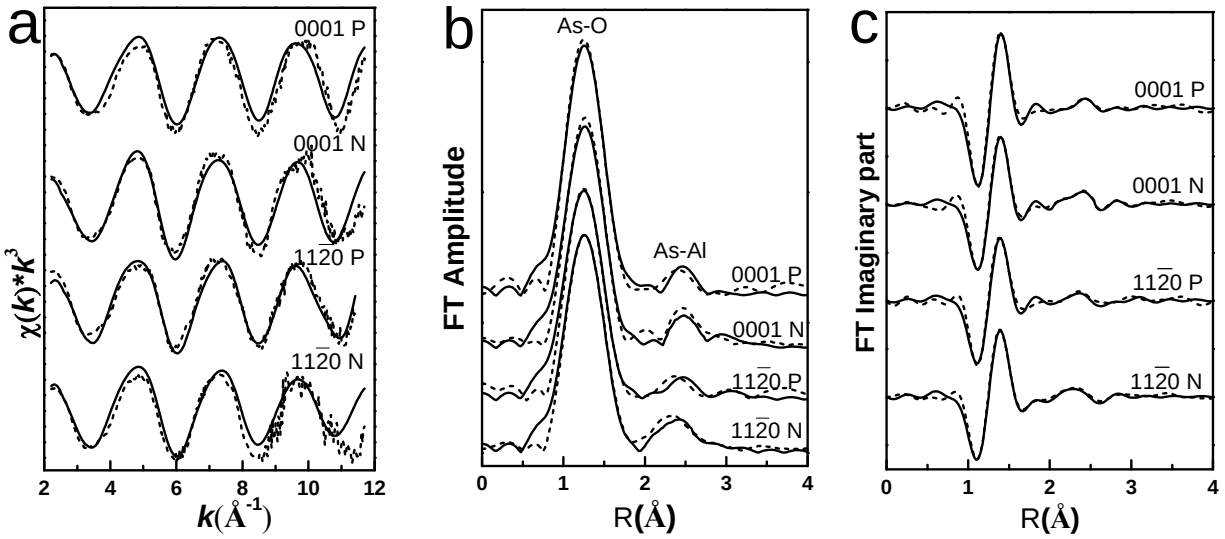


**Fig. 2**. (a) $k^3$-weighted GI-EXAFS, (b) Fourier transformed (FT) spectra, and (c) imaginary part of FT spectra of arsenate adsorption on α-$Al_2O_3$ (0001) and (11$\bar{2}$0) planes measured using two scan modes [electric vector parallel (P) and normal (N) to the substrate]. The dashed lines are the experimental spectra, while the solid lines are fitting curves. The peak positions are uncorrected for phase shifts.

**Table 2**. GI-EXAFS measured structural parameters of arsenate adsorption on α-$Al_2O_3$ (0001) and (11$\bar{2}$0) single-crystal planes*

| Shell | Type of neighbor | *CN* | *R*(Å) | *DW*($\sigma^2$) | $\Delta E_0$(eV) | *Residual*** (%) |
|---|---|---|---|---|---|---|
| **(0001) surface E-vector** parallel** | | | | | | |
| First | O | 4.0± 0.2 | 1.68± 0.005 | 0.002±0.001 | | |
| Second | Al | 1.5± 0.3 | 3.11± 0.02 | 0.004±0.001 | 2.23 | 10.2 |
| | Al | 0.7± 0.2 | 3.32± 0.03 | 0.007±0.002 | | |
| **(0001) surface E-vector normal** | | | | | | |
| First | O | 4.0± 0.2 | 1.69± 0.005 | 0.003±0.001 | | |
| Second | Al | 2.9± 0.6 | 3.12± 0.02 | 0.005±0.001 | 3.70 | 11.3 |
| | Al | 4.2± 0.8 | 3.35± 0.03 | 0.006±0.003 | | |
| **(11$\bar{2}$0) surface E-vector parallel** | | | | | | |
| First | O | 4.1± 0.2 | 1.68± 0.005 | 0.003±0.001 | | |
| Second | Al | 1.4± 0.3 | 3.03± 0.02 | 0.005±0.002 | 3.45 | 11.4 |
| | Al | 0.4± 0.1 | 3.19± 0.03 | 0.007±0.003 | | |
| **(11$\bar{2}$0) surface E-vector normal** | | | | | | |
| First | O | 3.9± 0.2 | 1.69± 0.005 | 0.002±0.001 | 4.65 | 11.0 |
| Second | Al | 3.7± 0.7 | 3.05± 0.02 | 0.006±0.002 | | |

| | | | | |
|---|---|---|---|---|
| | Al | 2.6± 0.6 | 3.22± 0.03 | 0.006±0.003 |

* The listed parameters (*CN*, coordination number; *R*, interatomic distance; $\sigma^2$, Debye-Waller factor) reflected the final best fit.

** E-vector, electric vector.

*** Residual, gives a measure of the agreement between experimental and theoretical FT curves. All Residuals are < 12%, indicating reliable fits.

An obvious difference in $CN_{\text{As-Al}}$ was observed from the same sample between the two scan modes (see Table 2), resulting from the polarization dependence of As-Al bonds. Different to the $CN_{iso}$ determined by standard powder EXAFS, the polarized coordination number ($CN_{pol}$) obtained from GI-EXAFS varies with the angle between the incident electric vector and the bond (Waychunas et al., 2005). The polarization dependence allows a maximum of $CN_{pol}$ when the bond parallel to the direction of electric vector, and a near-zero value would appear when the bond normal to the electric vector in the GI-EXAFS measurement. For instance, Fitts *et al.* presented that the $CN_{pol}$ of Cu-Si bond on $SiO_2$ (0001) surface in monodentate complex was 0.3 when the electric vector parallel to the substrate (Fitts et al., 1999). It was also reported that a zero $CN_{pol}$ value of Co-O bond occurred in an on-top complex of Co (II) adsorbed on α-$Al_2O_3$ (0001) surface when the bond was absolutely normal to the electric vector (Shirai et al., 1992; Shirai et al., 1994). The difference of $CN_{\text{As-Al}}$ between both polarized scans can be used to deduce the polar angle ($\phi$, angle between the As-Al vector and the substrate normal), and to determine the stereostructure of each surface complex. For the two scan modes (electric vector parallel and perpendicular to the support plane), the relationships between the coordination numbers of a polarized EXAFS measurement ($CN_{pol}$) and that of isotropic EXAFS ($CN_{iso}$) are $CN_{pol}^{\perp} = CN_{iso} \times 3cos^2\phi$ and $CN_{pol}^{II} = \frac{3}{2} CN_{iso} \times sin^2\phi$, respectively (Manceau et al., 2002; Waychunas et al., 2005). Based on the two equations, the polar angles ($\phi$) of BB complex obtained from GI-EXAFS fitting were 45°±8° on (0001) surface and 36°±6° on $(11\bar{2}0)$ surface, while the experimental $\phi$ of MB

complex on (0001) surface and MM complex on $(11\bar{2}0)$ surface were 33°±8° and 18°±11° respectively. The discrepancies between experimental and DFT-calculated polar angles (see Table 3) were less than 10°, indicating that a good estimation of the polar angles was obtained.

*3.2. DFT calculation*

$HAsO_4^{2-}$ is the dominant species of arsenate under pH 7.0 (i.e., the GI-EXAFS experimental condition) (Sadiq, 1997), and hence was used in the DFT calculation to determine the adsorption site preference. EXAFS signal is less influenced by the hydrogen atoms than by the heavier elements around the absorbing atoms, and thus hydrogen atoms are normally not included in analyses of EXAFS data. Here, we used DFT calculation to identify the protonation state of adsorbed arsenate. Monodentate binuclear (MB) and bidentate binuclear (BB) complexes are the two typical structures of arsenate adsorbed on the (0001) surface (see Fig. 3). On the $(11\bar{2}0)$ surface, there are two kinds of unsaturated oxygen sites, monodentate-terminal and bidentate-bridging O sites, which may be potentially formed the reactive sites. Arsenate would be bonded as monodentate mononuclear (MM) and bidentate binuclear (BB) structures at the terminal oxygen sites (Fig. 3), while a bidentate mononuclear (BM) adsorption mode may be potentially produced at the bridging oxygen sites (Fig. S5a). However, the calculated BM adsorption mode yielded an As-Al distance of 2.75 Å (see the Supporting Information), much smaller than the distance obtained from experimental GI-EXAFS measurement, which confirmed the fact that the twofold bridging oxygen site is less active than the high coordination-unsaturated terminal oxygen site at the $\alpha$-$Al_2O_3$ $(11\bar{2}0)$ surface. Outer-sphere adsorption of arsenate on $\alpha$-$Al_2O_3$ at pH 5 has been reported (Catalano et al., 2008). It is well known that the surface complexation of arsenate on metal-(hydr)oxides is significantly affected by pH. In our previous study of arsenate adsorption on anatase $TiO_2$ surfaces (He et al., 2009), we also found that the as pH decreased to 5.5, outer-sphere

adsorption became thermodynamically favorable. However, there was no evidence indicating the occurrence of outer-sphere adsorption of arsenate on α-$Al_2O_3$ surfaces under pH 7. Our DFT calculation showed that the As-Al distances would be ~5 Å in outer-sphere Al-$AsO_4$ complexes (Fig. S5b), however, no effective signals were observed more than 4 Å away from the As atom in the GI-EXAFS spectra (see Fig. S2). Furthermore, outer-sphere H-bonded adsorption of arsenate on α-$Al_2O_3$ surfaces [e.g., -251.5 kJ/mol on (0001) surface] was more thermodynamically unfavorable than the inner-sphere adsorption (-434.7 and -584.3 kJ/mol, see Table 3). This result indicated that arsenate adsorbed on the α-$Al_2O_3$ surfaces mainly as inner-sphere complexes under the neutral pH condition. Therefore, in order to directly compare calculated results with experimental data, complexation at the bridging oxygen sites on $(11\bar{2}0)$ surface and outer-sphere adsorption were excluded from the theoretical analysis and discussion.

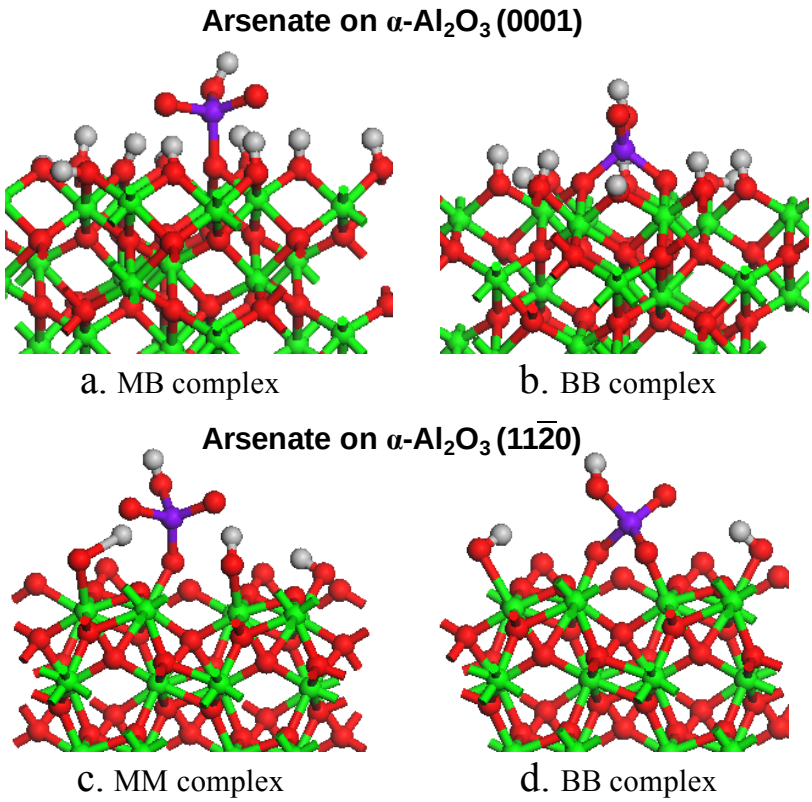


**Fig. 3.** DFT-calculated structures of arsenate adsorbed on α-$Al_2O_3$ (0001) and $(11\bar{2}0)$ surfaces. Purple, green, red, and gray circles denote arsenic, aluminum, oxygen, and hydrogen atoms, respectively.

Adsorption on the (0001) facet (-434.7 kJ/mol for monodentate complexes and -584.3 kJ/mol for bidentate complexes) were generally energetically more favorable than that on the $(11\bar{2}0)$ facet (-172.7 kJ/mol for monodentate complexes and -339.5 kJ/mol for bidentate complexes), indicating that the (0001) facet exhibited a higher affinity toward arsenate. The spectral and computational results showed that the polar angles of monodentate and bidentate complexes on the (0001) surface were respectively 10~20°greater than that on the $(11\bar{2}0)$ surface (see Table 3). The result suggested that a relatively large polar angle was more favorable for arsenate stabilized on α-$Al_2O_3$ surfaces. It can be also noted that the DFT-calculated As-O distances for the Al-$AsO_4$ surface complexes (1.71 Å) were generally slightly longer than the experimentally measured values (1.69 Å). This phenomenon was also observed in the adsorption of arsenite on Fe-(hydr)oxides (Zhang et al., 2005). This difference between experimental and theoretical values may be due to the theoretical underestimation of solvent effect from COSMO model (Costentin et al., 2004; Tossell, 2005). However, we expect that this artifact does not affect the relative stability of the adsorption modes and their complexation properties.

**Table 3.** DFT-calculated interatomic distances (Å), polar angles (º) and binding energies (Δ*E*) of arsenate adsorbed on α-$Al_2O_3$ surfaces

| Bond | As-O(H) | | | | Average | As- Al | | Average | Polar angle* | | Average | ΔE** (kJ/mol) |
|---|---|---|---|---|---|---|---|---|---|---|---|---|
| MB-(0001)-$HAsO_4^{2-}$ | 1.69 | 1.69 | 1.73 | 1.75 | 1.71 | 3.14 | 3.45 | 3.30 | 30 | 30 | 30 | -434.7 |
| BB-(0001)-$HAsO_4^{2-}$ | 1.69 | 1.71 | 1.72 | 1.74 | 1.71 | 2.98 | 3.17 | 3.07 | 42 | 40 | 41 | -584.3 |
| MM-$(11\bar{2}0)$-$HAsO_4^{2-}$ | 1.68 | 1.69 | 1.74 | 1.77 | 1.72 | 3.21 | — | 3.21 | 10 | — | 10 | -172.7 |
| BB-$(11\bar{2}0)$-$HAsO_4^{2-}$ | 1.69 | 1.70 | 1.72 | 1.75 | 1.71 | 3.01 | 3.13 | 3.07 | 33 | 30 | 32 | -339.5 |

* Polar angle is the angle between the surface normal and the interatomic As-Ti vector direction.

** $\Delta E$ were calculated as $\Delta E = E_{tot}(\text{Al-AsO}_4)$- [$E_{tot}$(arsenate) + $E_{tot}(\alpha\text{-Al}_2\text{O}_3)$], where $E_{tot}(\text{Al-AsO}_4)$ was the total energy of Al-$AsO_4$ adsorption complex, $E_{tot}$(arsenate) and $E_{tot}(\alpha\text{-Al}_2\text{O}_3)$ were the total energy of arsenate molecule and $\alpha$-$Al_2O_3$ cluster, respectively. The structures of non-adsorbed arsenate were optimized in a periodic box with a side length of 10 Å (Ojamae et al., 2006).

## 4. Conclusions

The spectral and computational results showed that arsenate primarily bonded as inner-sphere MB and BB complexes on the (0001) surface of $\alpha$-$Al_2O_3$, and MM and BB complexes on the $(11\bar{2}0)$ surface. The orientational polar angles on the (0001) surface were commonly 10~20° greater than that on the $(11\bar{2}0)$ surface for both monodentate and bidentate complexes. The DFT calculation showed that the (0001) surface exhibited a stronger affinity toward arsenate, suggesting that the large polar angle was more favorable for arsenate stabilization. The dominant bonding modes of arsenate on the two planes of $\alpha$-$Al_2O_3$ were identified as bidentate binuclear structures.

The combination of GI-EXAFS and DFT calculation facilitates the direct identification of adsorbed species on different exposed crystal planes of the mineral. Our results demonstrated the arsenate complexes on different crystal planes, which may be regarded as one single adsorption structure from the measurements based on powder substrates, exhibited an obvious difference in stability. This unambiguous characterization suggested a potential development to predict the fate and transport of arsenic in aluminum-bearing soils, sediments, and water treatment systems that should take into account the contributions from different crystal surfaces.

**Acknowledgement.** The study was supported by NNSF of China (21377003 and 21207151), and the special fund of State Key Joint Laboratory of Environment Simulation and Pollution Control (12L02ESPC). We thank SSRF for providing the beam time and Dr. Xiangjun Wei for help in GI-EXAFS data collection and analysis. We thank the Supercomputing Center of the Chinese

Academy of Sciences for providing access to the Materials Studio software.

## Appendix A. Supplementary data

Supplementary data to this article can be found online at

## References

Ankudinov, A. L., Ravel, B., Rehr, J. J., Conradson, S. D., 1998. Real-space multiple-scattering calculation and interpretation of x-ray-absorption near-edge structure. Phys. Rev. B, 58(12): 7565-7576.

Arai, Y., Elzinga, E. J., Sparks, D. L., 2001. X-ray absorption spectroscopic investigation of arsenite and arsenate adsorption at the aluminum oxide-water interface. J. Colloid Interface Sci., 235(1): 80-88.

Catalano, J. G., Park, C., Fenter, P., Zhang, Z., 2008. Simultaneous inner- and outer-sphere arsenate adsorption on corundum and hematite. Geochim. Cosmochim. Acta, 72(8): 1986-2004.

Catalano, J. G., Trainor, T. P., Eng, P. J., Waychunas, G. A., Brown Jr, G. E., 2005. CTR diffraction and grazing-incidence EXAFS study of U(VI) adsorption onto $\alpha$-$Al_2O_3$ and $\alpha$-$Fe_2O_3$ (1102) surfaces. Geochim. Cosmochim. Acta, 69(14): 3555-3572.

Costentin, C., Robert, M., Saveant, J. M., 2004. Stepwise and concerted electron-transfer/bond breaking reactions. Solvent control of the existence of unstable $\pi$ ion radicals and of the activation barriers of their heterolytic cleavage. J. Am. Chem. Soc., 126(51): 16834-16840.

Daniels, B. G., Lindsay, R., Thornton, G., 2001. A review of quantitative structural determinations of adsorbates on metal oxide surfaces. Surf. Rev. Lett., 8(1-2): 95-120.

Delley, B., 1990. An all-electron numerical-method for solving the local density functional for

polyatomic-molecules. J. Chem. Phys., 92(1): 508-517.

Delley, B., 1995. DMol, a standard tool for density functional calculations: review and advances. In: Seminario, J.M.P., P. (Ed.), Theoretical and Computational Chemistry. Elsevier, pp. 221-254.

Delley, B., 2000. From molecules to solids with the DMol(3) approach. J. Chem. Phys., 113(18): 7756-7764.

Duarte, G. et al., 2012. As(III) immobilization on gibbsite: investigation of the complexation mechanism by combining EXAFS analyses and DFT calculations. Geochim. Cosmochim. Acta, 83: 205-216.

Fitts, J. P. et al., 1999. Grazing-incidence XAFS investigations of Cu(II) sorption products at α-$Al_2O_3$-water and α-$SiO_2$-water interfaces. J. Synchrotron. Radiat., 6: 627-629.

Furnare, L. J., Vailionis, A., Strawn, D. G., 2005. Polarized XANES and EXAFS spectroscopic investigation into copper(II) complexes on vermiculite. Geochim. Cosmochim. Acta, 69(22): 5219-5231.

Grafe, M., Sparks, D. L., 2005. Kinetics of zinc and arsenate co-sorption at the goethite-water interface. Geochim. Cosmochim. Acta, 69(19): 4573-4595.

Grafe, M., Tappero, R. V., Marcus, M. A., Sparks, D. L., 2008. Arsenic speciation in multiple metal environments: I. Bulk-XAFS spectroscopy of model and mixed compounds. J. Colloid Interface Sci., 320(2): 383-399.

Hass, K. C., Schneider, W. F., Curioni, A., Andreoni, W., 1998. The chemistry of water on alumina surfaces: Reaction dynamics from first principles. Science, 282(5387): 265-268.

Hay, P. J., Wadt, W. R., 1985. Abinitio effective core potentials for molecular calculations - potentials for K to Au including the outermost core orbitals. J. Chem. Phys., 82(1): 299-310.

He, G., Pan, G., Zhang, M., 2011. Studies on the reaction pathway of arsenate adsorption at water-$TiO_2$ interfaces using density functional theory. J. Colloid Interface Sci., 364(2): 476-481.

He, G., Zhang, M., Pan, G., 2009. Influence of pH on initial concentration effect of arsenate adsorption on $TiO_2$ surfaces: thermodynamic, DFT, and EXAFS Interpretations. J. Phys. Chem. C, 113(52): 21679-21686.

Hellman, A., Gronbeck, H., 2009. First-Principles Studies of $NO_x$ Chemistry on $Ag_n/\alpha$-$Al_2O_3$. J. Phys. Chem. C, 113(9): 3674-3682.

Inada, Y., Orita, H., 2008. Efficiency of numerical basis sets for predicting the binding energies of hydrogen bonded complexes: Evidence of small basis set superposition error compared to Gaussian basis sets. J. Comput. Chem., 29(2): 225-232.

Jing, C., Liu, S., Patel, M., Meng, X., 2005. Arsenic leachability in water treatment adsorbents. Environ. Sci. Technol., 39(14): 5481-5487.

Klamt, A., 1995. Conductor-like screening model for real solvents - a new approach to the quantitative calculation of solvation phenomena. J. Phys. Chem., 99(7): 2224-2235.

Klamt, A., Schuurmann, G., 1993. Cosmo - a new approach to dielectric screening in solvents with explicit expressions for the screening energy and its gradient. J. Chem. Soc., Perkin Trans. 2(5): 799-805.

Klockenkämper, R., 1997. Total reflection X Ray Fluorescence Analysis. Wiley, New York

Lockwood, G. K., Zhang, S. H., Garofalini, S. H., 2008. Anisotropic dissolution of α-Alumina (0001) and (1120) surfaces into adjoining silicates. J. Am. Ceram. Soc., 91(11): 3536-3541.

Makov, G., Payne, M. C., 1995. Periodic boundary-conditions in ab-Initio calculations. Phys. Rev. B, 51(7): 4014-4022.

373 Manceau, A., Lanson, B., Drits, V. A., 2002. Structure of heavy metal sorbed birnessite. Part III:
374 Results from powder and polarized extended X-ray absorption fine structure spectroscopy.
375 Geochim. Cosmochim. Acta, 66(15): 2639-2663.
376 Mason, S. E., Iceman, C. R., Tanwar, K. S., Trainor, T. P., Chaka, A. M., 2009. Pb(II) Adsorption on
377 Isostructural Hydrated Alumina and Hematite (0001) Surfaces: A DFT Study. J. Phys. Chem. C,
378 113(6): 2159-2170.
379 Mohan, D., Pittman, C. U., Jr., 2007. Arsenic removal from water/wastewater using adsorbents - A
380 critical review. J. Hazard. Mater., 142(1-2): 1-53.
381 Montanari, B., Civalleri, B., Zicovich-Wilson, C. M., Dovesi, R., 2006. Influence of the
382 exchange-correlation functional in all-electron calculations of the vibrational frequencies of
383 corundum ($\alpha$-$Al_2O_3$). Int. J. Quantum Chem., 106(7): 1703-1714.
384 Ojamae, L., Aulin, C., Pedersen, H., Kall, P. O., 2006. IR and quantum-chemical studies of carboxylic
385 acid and glycine adsorption on rutile $TiO_2$ nanoparticles. J. Colloid Interface Sci., 296(1):
386 71-78.
387 Oremland, R. S., Stolz, J. F., 2003. The ecology of arsenic. Science, 300(5621): 939-944.
388 Perdew, J. P., Burke, K., Ernzerhof, M., 1996. Generalized Gradient Approximation Made Simple.
389 Phys. Rev. Lett., 77(18): 3865-3868.
390 Ranea, V. A., Schneider, W. F., Carmichael, I., 2008. DFT characterization of coverage dependent
391 molecular water adsorption modes on $\alpha$-$Al_2O_3$(0001). Surf. Sci., 602(1): 268-275.
392 Ressler, T., 1998. WinXAS: a program for X-ray absorption spectroscopy data analysis under
393 MS-Windows. J. Synchrot. Radiat., 5(2): 118-122.
394 Ressler, T., 2009. Manual WinXAS. Version 3.x,1992-2009. Department of Inorganic Chemistry.

395 Germany.
396 Roscioni, O. M., Dyke, J. M., Evans, J., 2013. Structural characterization of supported
397 $Rh^{I}(CO)_2/\gamma$-$Al_2O_3$ catalysts by periodic DFT calculations. J. Phys. Chem. C, 117(38):
398 19464-19470.
399 Sadiq, M., 1997. Arsenic chemistry in soils: An overview of thermodynamic predictions and field
400 observations. Water Air Soil Poll, 93(1-4): 117-136.
401 Shirai, M., Asakura, K., Iwasawa, Y., 1992. Anisotropic structure-analysis for cobalt oxides on
402 $\alpha$-$Al_2O_3$ (0001) by polarized total-reflection fluorescence extended X-ray absorption
403 fine-structure. Catal. Lett., 15(3): 247-254.
404 Shirai, M., Inoue, T., Onishi, H., Asakura, K., Iwasawa, Y., 1994. Polarized total-reflection
405 rluorescence exafs study of anisotropic structure-analysis for Co oxides on $\alpha$-$Al_2O_3$ (0001) as
406 model surfaces for active oxidation catalysts. J. Catal., 145(1): 159-165.
407 Singer, D. M. et al., 2012. Identification of Simultaneous U(VI) Sorption Complexes and U(IV)
408 Nanoprecipitates on the Magnetite (111) Surface. Environ. Sci. Technol., 46(7): 3811-3820.
409 Singer, D. M., Fox, P. M., Guo, H., Marcus, M. A., Davis, J. A., 2013. Sorption and redox reactions of
410 As(III) and As(V) within secondary mineral coatings on aquifer sediment grains. Environ. Sci.
411 Technol., 47(20): 11569-11576.
412 Tang, Y. Z., Reeder, R. J., 2009. Uranyl and arsenate cosorption on aluminum oxide surface. Geochim.
413 Cosmochim. Acta, 73(10): 2727-2743.
414 Tossell, J. A., 2005. Theoretical study on the dimerization of $Si(OH)_4$ in aqueous solution and its
415 dependence on temperature and dielectric constant. Geochim. Cosmochim. Acta, 69(2):
416 283-291.

417 Trainor, T. P., Fitts, J. P., Templeton, A. S., Grolimund, D., Brown, G. E., 2001. Grazing-incidence
418 XAFS study of aqueous Zn(II) sorption on α-$Al_2O_3$ single crystals. J. Colloid Interface Sci.,
419 244(2): 239-244.
420 van Genuchten, C. M., Addy, S. E. A., Pena, J., Gadgil, A. J., 2012. Removing arsenic from synthetic
421 groundwater with iron electrocoagulation: an Fe and As K-Edge EXAFS study. Environ. Sci.
422 Technol., 46(2): 986-994.
423 Walters, C. F., McCarty, K. F., Soares, E. A., Van Hove, M. A., 2000. The surface structure of α-$Al_2O_3$
424 determined by low-energy electron diffraction: aluminum termination and evidence for
425 anomolously large thermal vibrations. Surf. Sci., 464(2-3): L732-L738.
426 Wang, X. G., Chaka, A., Scheffler, M., 2000. Effect of the environment on α-$Al_2O_3$ (0001) surface
427 structures. Phys. Rev. Lett., 84(16): 3650-3653.
428 Waychunas, G. et al., 2005. Surface complexation studied via combined grazing-incidence EXAFS
429 and surface diffraction: arsenate on hematite (0001) and (1012). Anal. Bioanal. Chem., 383(1):
430 12-27.
431 Waychunas, G. A., Rea, B. A., Fuller, C. C., Davis, J. A., 1993. Surface-chemistry of Ferrihydrite .1.
432 EXAFS studies of the geometry of coprecipitated and adsorbed arsenate. Geochim.
433 Cosmochim. Acta, 57(10): 2251-2269.
434 Zhang, N. L., Blowers, P., Farrell, J., 2005. Evaluation of density functional theory methods for
435 studying chemisorption of arsenite on ferric hydroxides. Environ. Sci. Technol., 39(13):
436 4816-4822.
437
438